Optimization of T-shaped Suspension Magnetic Ring for Vertical Axis Wind Turbine

Zhu Jun [1], Song Dandan [1], Han Qiaoli [2], Wang Jinmei [1], Guanghua Li [1], and Li Shaolong [1]

[1] Department of Electrical Engineering
School of Electrical Engineering and Automation, Henan Polytechnic University, Jiaozuo, 454000, China
zhujunnd@163.com, 18625876973@163.com

[2] Department of Electrical Engineering
School of Energy and Transportation Engineering, Inner Mongolia Agricultural University
Hohehot Municipality, 010018, China
nmgtynxh@hotmail.com

Abstract ─ Aiming at realizing breeze startup, light wind power generation, a novel T-shaped group of passive magnetic bearing (PMB) with three rings high suspension characteristics was proposed to increase the utilization of wind energy and improve the suspension characteristics of passive bearings. The inner magnetic ring of the T-shaped magnetic ring group adopts an oblique 45° polarization method, which can simultaneously balance radial force and axial force with high suspension characteristics. The static characteristics of the T-shaped magnetic ring group are compared with the traditional double rings which dynamic disturbance characteristics were analyzed in three degrees of freedom (DOF) and the parameters are optimized to achieve the optimal suspension characteristics through methods of Taguchi, response surface with mathematical model. The study shows that the capacity of T-shaped magnetic ring group is 2.5 times which can balance axial force and radial force simultaneously with 40% increase in volume than the double ring. The capacity of T-shaped magnetic ring group is increased by 33.6% and the stiffness is increased by 33.7% after optimized, which meets the requirements of suspension characteristics. When the bearing is disturbed in 3 DOF operation, the stable running state of the bearing can still be maintained due to its self-stabilizing system. It provides a reference for the suspension characteristics of the vertical axis wind turbine suspension system.

Index Terms ─ 3 DOF, magnetic bearing, stability, T-shaped magnetic ring group.

I. INTRODUCTION

The performance of shafting components and the whole system are affected by bearing performance directly. Magnetic suspension bearings have the advantages of no friction, no wear and long service life which have broad application prospects [1-3]. At present, magnetic suspension technology has made achievements in flywheel energy storage, pump, Hydropower Synchronous Generator, hard disk drive, maglev train, medical [4-10] and so on. The introduction of suspension technology to the wind power generation system can reduce the starting torque and expand the utilization rate of wind energy.

In order to improve the suspension characteristics of PMB, the domestic and foreign scholars have done a lot of research on their polarization direction, geometry structure and dynamic characteristics. The rotor is suspended by a repulsive force to replace the mechanical bearings and can generate anti-disturbance suspension characteristics with the parallel magnetized permanent magnets installed on the rotor and stator respectively [11-12]. In view of the greater force of the change polarization method than the single polarization [13], the literature [14-15] proposed the continuous Halbach structure with high rigidity, but with high processing cost. A comparative study was made on the suspension characteristics of four different polarized directions in different geometric structure, in which the suspension characteristics of the rotating 90 degree polarization are the best, but the installation is difficult [16-17].

The structure of three-ring was presented with high stiffness and bearing capacity, but its system stability is poor [18-22]. In order to keep the balance of the suspension system in every degree of freedom, the axial force is balanced by the radial magnetic ring group and the axial magnetic ring group, but the cost increased [23].

For its dynamic characteristics, the physical mathematical model was established for a passive magnetic and the danger were studied arising from possible resonances when the natural frequencies of the device were near to the excitation frequencies [24]. Two novel nonlinear controllers were studied in reference

Submitted On: May 17, 2018
Accepted On: June 13, 2018

23 for single-biasing freedom with anti-interference performance. But only one degree of freedom control can be realized [25].

In order to realize the goal of "light wind start, breeze wind power generation" and solve the above problems, a novel T-shaped group of PMB with three rings which can balance axial and radial forces simultaneously and is suitable for vertical axis is proposed; which high-suspension features can reduce the starting torque of wind turbines and increase wind energy utilization. Compared with the traditional double ring bearing, the bearing capacity of the new three-ring T-shaped magnetic ring group is increased by 2.5 times and has sufficient self-stability.

II. STRUCTURE OF SUSPENSION SYSTEM

Magnetic suspension bearing is a kind of bearing that uses a magnetic field force to suspend the shaft. According to its working principle, it can be divided into active magnetic bearing, passive magnetic bearing and mixed magnetic bearing. The passive magnetic bearing can be divided into the whole passive magnetic bearing (superconductor, diamagnetic body) and the permanent magnetic bearing (PMB). In passive magnetic bearings, permanent magnetic bearings are commonly used.

According to the Earnshaw theorem, it is impossible to maintain a stable suspension in 6 degrees of freedom. The Laplace equation of static magnetic field is as follows:

$$\partial^2 W = 0, \tag{1}$$

$$\frac{\partial^2 W}{\partial_{X^2}} + \frac{\partial^2 W}{\partial_{Y^2}} + \frac{\partial^2 W}{\partial_{Z^2}} = 0. \tag{2}$$

Where W is the magnetostatic energy of the system. To make the system in a stable balance, the second-order derivative of the magnetostatic energy must be greater than zero:

$$\frac{\partial^2 W}{\partial_{X^2}} > 0, \frac{\partial^2 W}{\partial_{Y^2}} > 0, \frac{\partial^2 W}{\partial_{Z^2}} > 0. \tag{3}$$

Obviously, the two formulae of (2) and (3) cannot be satisfied at the same time. This means that in an external magnetic field with only permanent magnets, it cannot be stable in all the degrees. In the best case, stability can only be obtained in two degrees of freedom. In the other degree of freedom, electromagnetic force and other controllable forces, such as hydraulic pressure and friction must be introduced to achieve a stable balance T-shaped magnetic ring group.

The vertical axis suspension system with T-shaped magnetic ring group instead of traditional mechanical bearings is shown in Fig. 1. The lower magnetic ring balances the gravity of the system, the outer magnetic ring balances the radial force of the system, and the upper T-type magnetic ring group serves as a backup magnetic ring group to prevent the system from going up so as to ensure the stability of the system fundamentally.

When the inner magnetic ring is shifted to the left side, the left air gap decreases, but the magnetic density increases, and the inner magnetic ring is repelled to the right and restored to the equilibrium position. In order to make the kr/V reach the maximum, the square cross-section or square cross-section of the permanent magnet is selected usually.

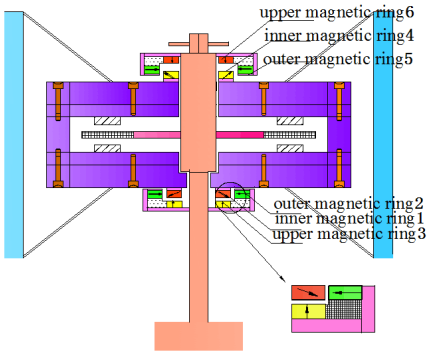

Fig. 1. Schematic diagram of vertical axis wind power generation system.

III. ANALYSIS AND CALCULATION OF MAGNETIC BEARINGS

A. Basic dimensions

The permanent magnetic material of the article is selected from NdFeB, whose Fe65%, Nd33%, B1.2%, and the maximum energy product can be as high as 400kJ/m3. Its outstanding performance makes it widely used. In order to ensure the maximum working capacity of the permanent magnet, the static analysis working point of the permanent magnet is stabilized near the maximum energy product and the proper bearing size is calculated by analyzing the demagnetization curve and the anti-magnetic curve of the NdFeB material.

The radial magnetization length of the permanent magnet is:

$$L_m = fkH_g L_g \sqrt{\frac{B_r}{H_C (BH)_{\max}}}. \tag{4}$$

f stands for magnetic resistance, usually between 1.1-1.5, k is the correction factor of the length of magnetic circuit in air which is equivalent to the length of air gap magnetic circuit, L_g is working air gap length, this paper takes 0.5mm, H_g is the air-gap magnetic field intensity, B_r is remanent magnetization, H_c is the coercive force, BH is the maximum magnetic energy product.

After the above calculation, the L_m is 10mm and the height of the magnetic ring is 10mm to ensure the maximum of kr/V.

B. Displacement in axial

The geometrical parameters of bearing have great

influence on the stiffness and capacity of passive magnetic bearing. The bearing capacity is an important parameter to measure the bearing, and the bearing capacity is proportional to the square of the magnetic density of the air gap and the air gap area between the magnetic rings. Reasonable magnetic circuit and geometric parameters play a key role in bearing capacity. Its size parameters are shown in Fig. 2.

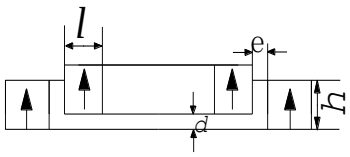

Fig. 2. The basic size of the magnetic ring.

Since the inner and outer magnetic rings are concentric magnetic rings and axially symmetrical. So the permanent magnet bearing radial force is 0, the axial force is:

$$F_x = \frac{-J_0^2}{2\pi\mu_0} p\{2\phi(d) - \phi(d+h) - \phi(d-h)\}. \quad (5)$$

In the formula:

$$\phi(z) = \left\{(2l+e)Arctg\frac{2l+e}{z} - 2(l+e)Arctg\frac{2l+e}{z} + eArctg\frac{e}{z} - \frac{z}{2}\left[\ln(2l+e)^2 + z^2 - 2\ln\left(l+e\right)^2 + \ln(e^2+z^2)\right]\right\}. \quad (6)$$

Where p is the average perimeter of the magnetic bearing, h and l are the height and width of the permanent magnet, e is the gap, d is the axial offset distance, and J_0 is the magnetic polarization of the surface of the permanent magnet.

The stiffness may change the natural frequency and other dynamic characteristics of the system which is related to the bearing geometry, working environment and other factors. According to the Enshaow theorem, the higher the stiffness is, the higher the stability of the bearing is. The radial stiffness is half of the axial stiffness, so the magnitude of the axial stiffness represents the support characteristics of the magnetic bearing. The formula is as follows:

$$K_r = \frac{-J_0^2}{8\pi\mu_0} p\left[2\rho(d) - \rho(d+h) - \rho(d-h)\right]. \quad (7)$$

In the formula:

$$\rho(z) = \ln\frac{[(2l+e)^2 + z^2][e^2+z^2]}{[(l+e)^2+z^2]^2}. \quad (8)$$

Axial stiffness:

$$K_x = -2K_r. \quad (9)$$

In the center position (d=0):

$$K_r = \frac{J_0^2}{4\pi\mu_0} p\left[\rho(h) - \rho(0)\right]. \quad (10)$$

C. T-shaped magnetic ring group

Traditional magnetic rings use one pair of radial magnetic rings for generating radial force or one pair of axial magnetic rings for generating axial force. Considering the economics of permanent magnets, a T-shaped magnetic ring group was proposed. Compared with the traditional radial superposed double-ring magnetic bearing, the three-ring T-shaped magnetic ring group adds a magnetic ring that is in conformity with the inner magnetic ring specification and uses an oblique downward 45° polarization direction below the original double-ring magnetic ring group. It increases the magnetic density and area near the inner ring with greater capacity and stiffness.

Figure 3 (a) is the overall diagram of its structure and Fig. 3 (b) is a polarization section; the lower magnetic ring is polarized upward, the outer magnetic ring is inward polarization, the inner magnetic ring is inclined downward 45 degrees, the inner ring is suspended in the axial and radial force of the two magnetic rings. Figure 3 (c) is the cross section of the magnetic force line with the trend of its magnetic force line can be seen.

The bearing capacity of the new magnetic ring group is 2.5 times higher than the double ring with its unique structure, as shown in Fig. 4. The g_2 of the upper standly magnetic ring is 14mm which generates 80N force in a stable state. The bearing capacity of the new T-shaped magnetic ring group can provide 267N bearing capacity in the static state, but the actual operation of the need to provide the wind turbine system and its components and the gravity of the upper magnetic gravity repulsion is 280N, so the structural parameters need to be optimized.

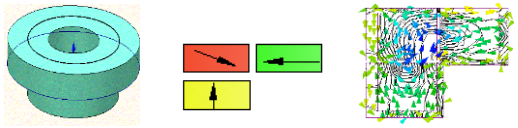

Fig. 3. Schematic diagram of T type magnetic ring. (a) Structure of T-shaped magnetic ring, (b) polarized section, and (c) section of magnetic line.

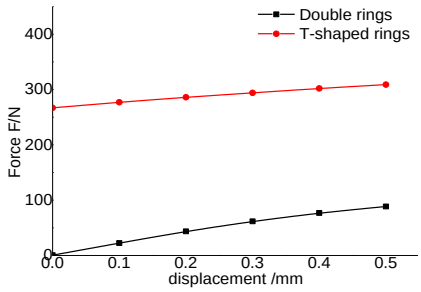

Fig. 4. Comparison of the bearing capacity of the two magnetic rings.

IV. OPTIMIZATION OF BEARING

A. Optimization of magnetic ring thickness *l* and air gap g_1

The suspension characteristic of the magnetic bearing is related to its geometric parameters. In this paper, four parameters of magnetic ring thickness A (l), magnetic ring height B (h) and air gap C (g_1) and D (g_2) between rings are taken as the factors and the multi-objective optimization design of magnetic bearing is carried out.

The influence of the four parameters on the bearing capacity F and the stiffness K of the passive magnetic bearing is studied and the quality characteristic of the magnetic bearing is optimized through optimization. That is to say, it has high bearing capacity and high stiffness. In the orthogonal test, the optimized target is called the quality characteristic, the condition that affects the quality characteristic is called factor and the value of the factor is called the level of the factor. The factor and the level of the factor are as shown in Table 1.

Table 1: The factors and the value of its level

Variables	A/mm	B/mm	C/mm	D/mm
Factorlevel1	9	9	0.4	0.8
Factorlevel2	10	10	0.5	1
Factorlevel3	11	11	0.6	1.2
Factorlevel4	12	12	0.7	1.4

Each optimization variable takes 4 factor levels and combination of the orthogonal experiment was carried out. Traditional analysis variables need to do $4^4 = 256$ times experiments, while Taguchi method establishes the experimental analysis matrix, which requires only 16 times finite element analysis and its specific orthogonal table is shown in Table 2.

Table 2: The actual value and result of the orthogonal table of 4 variables

N	A/mm	B/mm	C/mm	D/mm	F/N	K/(N/mm)
1	9	9	0.4	0.8	289.6	413.8
2	9	10	0.5	1	303.5	337.2
3	9	11	0.6	1.2	314.7	286.1
4	9	12	0.7	1.4	322.8	248.3
5	10	9	0.5	1.2	325.5	295.9
6	10	10	0.4	1.4	357.1	274.7
7	10	11	0.7	0.8	328.0	468.5
8	10	12	0.6	1	358.1	397.9
9	11	9	0.6	1.4	351.9	270.7
10	11	10	0.7	1.2	358.3	325.8
11	11	11	0.4	1	396.1	440.2
12	11	12	0.5	0.8	394.4	563.5
13	12	9	0.7	1	357.5	397.2
14	12	10	0.6	0.8	388.1	554.5
15	12	11	0.5	1.4	436.2	335.5
16	12	12	0.4	1.2	360.0	327.3

B. The proportion of factor level on quality characteristics

Analyzing the influence of 4 factors on quality characteristics of proportion, such as factor A in level factor 2 effect on the F can be solved as follow:

$$F_{A2} = \frac{1}{4} \times \left(F_{A25} + F_{A26} + F_{A27} + F_{A28} \right). \tag{11}$$

The effect of each factor level on factors A, B, C and D are shown in the following Tables 3, 4.

Table 3: Bearing capacity under different level factors

Factor Level	Force F/N			
	A/mm	B/mm	C/mm	D/mm
1	307.6	331.2	350.7	350.0
2	342.2	351.8	364.9	353.8
3	375.2	368.7	353.2	339.7
4	385.5	358.8	341.6	367.0

Table 4: Bearing stiffness under different level factors

Factor Level	Stiffness K/(N/mm)			
	A/mm	B/mm	C/mm	D/mm
1	321.3	344.4	364.0	500.1
2	359.3	373.0	383.0	393.1
3	400.0	382.6	377.3	308.8
4	403.6	384.3	360.0	282.3

C. The proportion of factors affecting the quality characteristics

The average values of bearing capacity $\overline{F}$ and stiffness $\overline{K}$ can be obtained from the results of 16 groups of orthogonal experiments in Table 2. The effects of four variables, A, B, C and D on multi-objective optimization are analyzed, as shown in Table 4.

The influence of four factors A, B, C, D on the bearing capacity F and stiffness K is analyzed, such as the influence of factor A on the bearing capacity F, and the formula is as follows:

$$S_{SB} = 4\sum_{i=1}^{4} \left(F_{Ai} - \overline{F} \right)^2. \tag{12}$$

Where F_{Ai} is the average of the bearing capacity F under the influence factor A and the Factor level i; $\overline{F}$ is the average value of the bearing capacity.

Table 5: The influence of four variables on two quality characteristics

Factor	F/N		K/(N/mm)	
	S_{SB}	Percentage	S_{SB}	Percentage
A	14881	72%	18046	13%
B	3040	15%	4081	3%
C	1101	5%	1423	1%
D	1533	7%	115546	83%
SUM	20556	1.00	139097	1.00

D. Analysis of results

In order to know the influence of each level factor on the bearing capacity F and the stiffness K intuitively, Tables 3, 4 is used for graphic processing which is shown in Fig. 5.

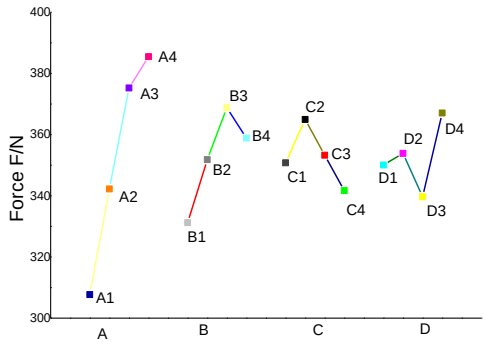

(a) Analysis of bearing capacity

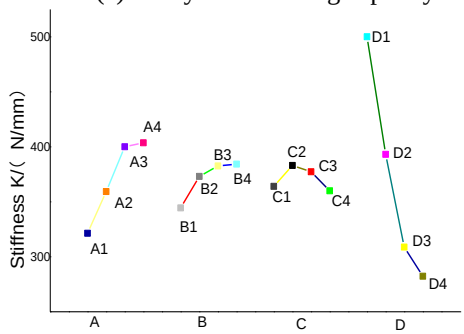

(b) Analysis of stiffness

Fig. 5. Influence of each factor level on bearing capacity F and stiffness K.

It can be seen from Fig. 5 that the maximum combination of the bearing capacity is $A_4B_3C_2D_4$, while the maximum combination of the stiffness K is $A_4B_4C_2D_1$. It can be seen from Table 5 that the influence factor A has the most influence and factor C has the least influence on the force, while the influence factor D has the most influence and factor C has the least influence on the stiffness.

To achieve multi-objective optimization, the final value of A_4C_2 can be determined by Taguchi algorithm. Since the choice of B or D has a greater impact on the bearing capacity F and the stiffness K. The specific values of B and D are verified and analyzed by the following optimization methods.

E. Optimization of magnetic ring height *h* and magnetic ring gap g_2

The second order model of the response output and the variable response factor were proposed by selecting the experimental design scheme which using Graphical method and analysis method to find out the optimization setting of independent variables. This method is a traditional statistical method to solve multivariate problems. An appropriate mathematical model is firstly established by experimental data, the function between objective function and variable is usually established by using second order function:

$$y = \beta_0 + \beta_1 x_1 + \beta_2 x_2 + \beta_{11} x_1^2 + \beta_{22} x_2^2 + \beta_{12} x_1 x_2 + \varepsilon. \quad (13)$$

Where y is the response function of magnetic bearing capacity F or stiffness K, β is the undetermined coefficient, ε is fitting error, x_1 and x_2 are the height of magnetic ring B(h), the upper and lower magnetic loop D (g_2), respectively.

The size of the magnetic ring height B(h) affects the magnetic flux density of the magnetic ring. In the unsaturated zone, the magnetic density increases as the material increases. The size of the air gap D(g_2) affects the magnetic flux density and magnetic flux leakage. In a suitable air gap, the magnetic density increases as the air gap decreases. Outside the reasonable range, the magnetic flux leakage increases and the magnetic flux density decreases as the air gap increases [26]. The magnetic density and air gap area plays a decisive role in the bearing capacity of the passive suspension bearing, so the optimal solution can be obtained through scientific and rigorous optimization. From the above optimization analysis, it can be seen that when B belongs to B_1 - B_3 and D belongs to D_1 - D_3 can achieve the optimal target, the range of independent variables are:

$$11\text{mm} < B(l) < 12\text{mm},$$
$$0.8\text{mm} < D(g2) < 1.4\text{mm}.$$

By using the central group design method, the values of independent variables are encoded separately. The center point is set to ensure the uniform accuracy of the predicted values of the entire experimental area. The experimental scheme and results are obtained as follows in Table 6.

Table 6: Design and results of experimental

N	Variables		Encod		F/N	K/(N/mm)
	B(h)	D(g2)	X1	X2		
1	12.0	1.1	1	0	443.5	443.5
2	12.0	0.8	1	-1	429.1	613.1
3	11.0	0.8	-1	-1	410.7	586.7
4	11.0	1.4	-1	1	436.2	335.5
5	11.5	0.8	0	-1	420.0	600.0
6	11.5	1.1	0	0	434.0	434.0
7	12.0	1.4	1	1	454.8	349.8
8	11.5	1.4	0	1	445.1	342.4
9	11.0	1.1	-1	0	425.0	425.0

The 9 groups of orthogonal experimental results are obtained through the analysis of the finite element. The mathematical model of stiffness K and capacity F are estimated by the least square method as follows:

$$y_1 = 263.958\text{-}0.186197x_1 + 75.1742x_2 + 0.797271 x_1^2\text{-}16.6519x_2^2 + 0.336581x_1x_2, \quad (14)$$

$$y_2 = 1010.59 + 26.7892x_1\text{-}1105.58x_2 + 0.6500724 x_1^2 + 412.227x_2^2\text{-}20.0169x_1x_2. \quad (15)$$

Figure 6 is a curved surface map and a contour map that responds to the target and variable factor which can solve the best combination of factors. The slope size of response surface reflects the significant influence of interaction between two variables on the response value. The steeper the slope is, the more significant the interaction effects on the response value. On the contrary, it is not significant.

Figure 6 (a) is surface diagram formed by the force, magnetization height and air gap; 6 (b) is the contour map of the force, magnetization height and air gap. In Fig. 6 (b), the deepest part of the color indicates that the force is greater than 450N when H is between 11.75 and 12mm and the g_2 is between 12.5 and 1.4mm can reach the maximum capacity. Figure 6 (c) is surface diagram formed by the stiffness, magnetization height and air gap; 6 (d) is the contour map of the stiffness, magnetization height and air gap when the thickness belongs to 11.45-12mm and the gap belongs to 0.8-0.83mm, stiffness can reach the maximum. Through the analysis of Minitab, the overall solution of the response optimization is (x_1, x_2) = (12, 0.94).

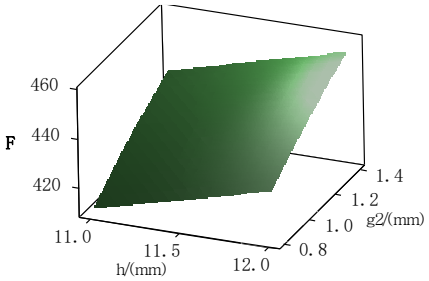

(a) Surface diagram formed by the force, height and air gap

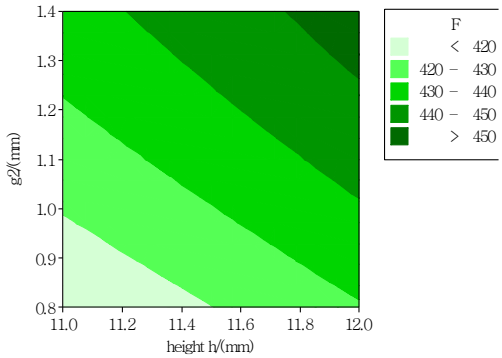

(b) The contour map of the force, height and air gap

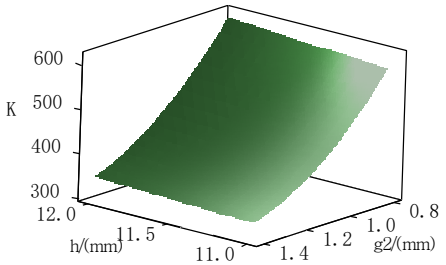

(c) Surface diagram formed by the stiffness, height and air gap

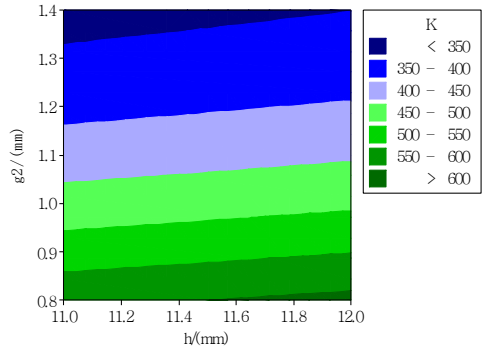

(d) The contour map of the force, height and air gap

Fig. 6. The surface and contour map of height and air gap and force and stiffness.

V. COMPARATIVE ANALYSIS

The parameters that affect the size of the magnet ring are optimized by two optimization methods. The geometric parameters are finally determined as follows: the thickness of the magnet ring A(l) is 12mm, the height of the magnet ring B(h) is 12mm, and the air gap C(g_1) is 0.5mm and D(g_2) is 0.93mm. The suspension characteristics before and after optimization are shown in Fig. 7. The direction of gravity acceleration is positive, and the displacement reference direction is set to negative direction when the inner magnetic ring is shifted upwards.

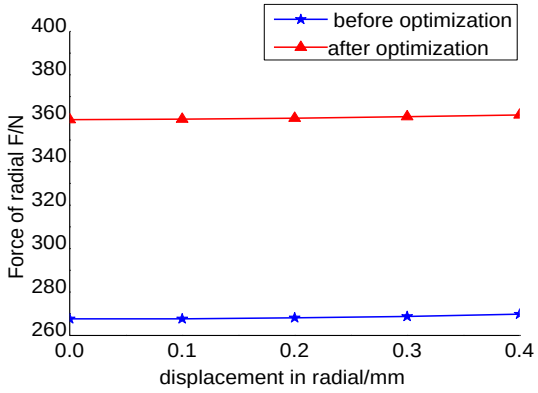

(a) Comparison of bearing capacity

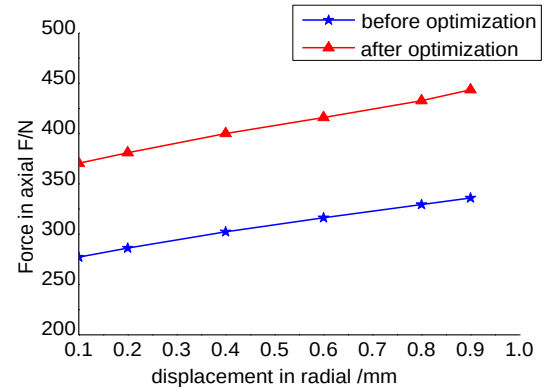

(b) Comparison of bearing capacity

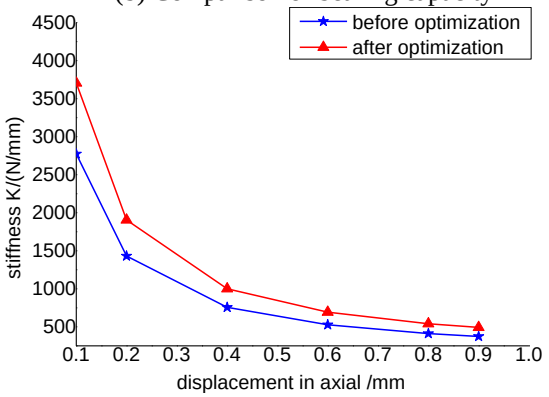

(c) Comparison of bearing stiffness

Fig. 7. Comparison of suspension characteristics.

According to the comparison and analysis of Fig. 7, the bearing capacity of the optimized passive bearing increased by 33.6% and the stiffness increased by 33.7%. Due to the need to provide a total of 280N for the gravity of the wind turbine system and its components and the repulsion of the upper magnetic ring, the optimization result meets the design requirements with a margin of 1.3 times.

VI. DYNAMIC CHARACTERISTICS

The dynamic characteristics of the bearing are derived from its equation of motion. Assuming that the bearing is balanced at z_0 and an interference is generated from the outside to cause a bearing disturbance $z_1(t)$. The equation of the bearing motion is:

$$z(t) = z_1(t) + z_0 . \tag{16}$$

The bearing suspension force is F_l and the bearing weight is mg. The motion equation of the bearing can be obtained in the vertical direction with interference:

$$m\frac{d^2 z_1}{dt^2} + c\frac{dz_1}{dt} + kz = F_1(z) - mg. \tag{17}$$

Where m is the bearing mass, c is the damping coefficient, and k is the stiffness factor. The maximum value of the damping condition is explained. The maximum amplitude of the damping is 0.1mm, and the amplitude gradually decreases due to the stability of the magnetic field. The initial values are: $z_1(0)=h$, $z_1'(0)=0$. h is the maximum displacement of the bearing from the equilibrium point, and the speed is 0 at this time. The equation can be reduced to a differential equation group:

$$\begin{cases} z_1 = f_1 \\ df_1 / dt = f_2 \\ df_2 / dt = \dfrac{1}{m} F_1(z) - g. \\ f_1(0) = h \\ f_2(0) = 0 \end{cases} \tag{18}$$

The system can operate efficiently and make full use of wind energy with its self-stability. The passive T-shaped magnetic ring group has no power electronic control device and the immunity to external disturbances is worth studying. The self-stability of the disturbance was investigated when the system was operated at 3 DOF which refer to the left and right directions in the X axis direction, the up and down directions in the Y axis direction, and the Z axis rotation.

When the inner magnetic ring is disturbed by the Z axis, it will offset the equilibrium position and generate an amplitude in the axial direction. The reduction of the air gap between the inner magnetic ring and the lower magnetic ring will cause the lower magnetic ring to generate a repulsive force to reduce the amplitude of the inner magnetic ring and return to a stable position gradually. The curve of speed change is shown in Fig. 8.

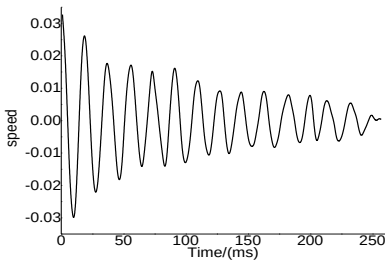

Fig. 8. Curve of speed (m/s).

VII. CONCLUSION

This paper presents a T-shaped group of PMB with three magnetic rings bearing for vertical axis wind power generation system. The structure has high suspension characteristics through the increase of magnetic flux density and section area and optimization of geometrical parameters. Research shows:

(1) The bearing capacity and stiffness of T-shaped group of PMB with three rings are 2.5 times of the double ring magnetic ring with better suspension characteristics, which is more suitable for adopting in the small wind turbine generator system.

(2) The geometric parameters of the magnetic ring have great influence on the suspension characteristics of the magnetic ring group. The thickness of the magnetic ring *l* has the greatest influence on the bearing capacity. The air gap g_2 between the upper and lower magnetic rings has the greatest influence on the stiffness. The capacity of T type magnetic ring group is increased by 33.6% and the stiffness is increased by 33.7% after optimized through methods of Taguchi, response surface with mathematical model, which meets the requirements of suspension characteristics.

(3) The T-shaped group of PMB with three magnetic rings provides enough axial repulsive force for the system with its novel structure and reasonable magnetization direction to balance the gravity and enough centripetal force of the system, so as to stabilize the system's disturbance in the radial direction. The upper T-shaped magnetic ring group is used as a spare magnetic ring group which ensures the stability of the system. When the bearing is disturbed in the three degree of freedom operation, the stable running state of the bearing can still be maintained due to its self-stabilizing system.

ACKNOWLEDGEMENTS

I would like to express my gratitude to all those who helped me during the writing of this thesis. My deepest gratitude goes first and foremost to Professor Zhujun, who has hosted many projects; key scientific and technological breakthrough projects in Henan Province: the research of low-speed direct-drive magnetic levitation axial flux wind turbine is conducted from September 2017 to September 2019 with its project number of 182102210052; Henan Colleges special funding for basic scientific research business expenses exploratory project: the vertical moving permanent magnet linear synchronous motor in meta information without sensing control key technology research is conducted from January 2015 to December 2018 with its project number of NSFRF140115. Key project of science and technology research of Henan Provincial Department of Dducation: the study on the theoretical study of the improved kalman filter permanent magnet synchronous motor without sensor control has been concluded from April 2014 to December 2014 with its project number of 12A470004. Also, my supervisor, for his constant encouragement and guidance; without his consistent and illuminating instruction, this thesis could not have reached its present form. Lastly my thanks would go to my beloved family for their loving considerations and great confidence in me all through these years. I also owe my sincere gratitude to my friends and my fellow classmates who gave me their help and time in listening to me and helping me work out my problems during the difficult course of the thesis.

REFERENCE

[1] Z. Weiyu, "Study on key technologies and applications of magnetic bearings", Transactions of China Electrotechnical Society, vol. 30, no. 12, pp. 11-20, 2015.

[2] Sunyang, "The design of flywheel energy storage system controller based on DSP+FPGA," *Hangzhou: Zhejiang University*, 2018.

[3] Liusijia, "A rotor position control system of the vertical magnetic bearing based on linear induction motors," *Beijin: Beijing Jiaotong University*, 2017.

[4] G. Goncalves Sotelo, "Magnetic bearing sets for a flywheel system," *IEEE Transactions on Applied Super-conductivity*, vol. 17, no. 2, pp. 2150-2153, 2007.

[5] R. Moser, "Optimization of repulsive passive magnetic bearings," *IEEE Transactions on Magnetics*, vol. 42, no. 8, pp. 2038-2042, 2006.

[6] G. H. Jang and J. S. Park, "Development of a highly efficient hard disk drive spindle motor with a passive magnetic thrust bearing and a hydrodynamic journal bearing," *Appl. Phys*., vol. 97, no. 10, pp. 507-507, 2005.

[7] X. Tang and Z. Yun, "The design of the magnetic and hydraulic suspension system on an axial blood pump and the analysis of its mechanical properties," *IEEE 2nd Advanced Information Technology, Electronic and Automation Control Conference (IAEAC), IEEE*, Chongqing, 2017.

[8] H. Silu, C. Hu, and H. Lingduo, "Current loop analysis of magnetic suspension controller for magnetic suspension bearing," *Information Technology, Networking, Electronic and Automation Control Conference, IEEE*, Chongqing, 2016.

[9] L. L. Zhang and J. H. Huang, "Stability analysis for a flywheel supported on magnetic bearings with delayed feedback control," *The Applied Computational Electromagnetics Society*, vol. 32, no. 8, pp. 642-649, 2017.

[10] J. J. Pérez-Loya, C. J. D. Abrahamsson, F. Evestedt, and U. Lundin, "Performance tests of a permanent magnet thrust bearing for a hydropower synchronous generator test-rig," *The Applied Computational Electromagnetics Society*, vol. 32, no. 8, pp. 407-411, 2017.

[11] P. Puentener, "Homopolar bearingless slice motor in temple design," *International Electric Machines and Drives Conference, IEEE*, Miami, 2017.

[12] G. Wu and X. Wang, "Design and analysis of a novel axial actively regulated slotless skew winding bearingless motor," *International Conference on Mechatronics and Automation (ICMA), IEEE*, Beijing, 2015.

[13] J.-P. Yonnet, G. Lemarquand, S. Hemmerlin, and

E. Olivier-Rulliere, "Stacked structures of passive magnetic bearings," *Appl. Phys*., vol. 70, pp. 6633, 1991.
[14] D. Kevin, "Stable levitation of a passive magnetic bearing," *IEEE Transactions on Magnetics*, vol. 49, no. 1, pp. 609-617, 2013.
[15] E. Marth, "A 2-D-based analytical method for calculating permanent magnetic ring bearings with arbitrary magnetization and its application to optimal bearing design," *IEEE Transactions on Magnetics*, vol. 50, no. 50, 7400308, 2014.
[16] N. Tănase, "Passive magnetic bearings for flywheel energy storage - Numerical design, passive magnetic bearings design," *International Conference on Applied and Theoretical Electricity*, Craiova, IEEE, 2014.
[17] J. Sun and D. Chen, "Stiffness measurement method of repulsive passive magnetic bearing in SGMSCMG," *IEEE Transactions on Instrumentation and Measurement*, vol. 62, no. 11, pp. 2960-2965, 2013.
[18] G. Goncalves Sotelo, "Magnetic bearing sets for a flywheel system," *IEEE Transactions on Applied Superconductivity*, vol. 17, no. 2 pp. 2150-2153, 2007.
[19] R. Ravaud, G. Lemarquand, and V. Lemarquand, "Halbach structures for permanent magnets bearings," *Prog. Electromagn*., vol. 14, pp. 263-277, 2007.
[20] R. Ravaud, "Force and stiffness of passive magnetic bearings using permanent magnets. Part 1: Axial magnetization," *IEEE Transactions on Magnetics*, vol. 45, no. 7, pp. 2996-3002, 2009.
[21] M. Alizadeh Tir, "Design of a new structure passive magnetic bearing with radial magnetization using FEM," *The 22nd Iranian Conference on Electrical Engineering, IEEE*, Tehran, 2014.
[22] M. Alizadeh Tir, "A novel structure of passive magnetic bearing with axial magnetization," *The 5th Power Electronics, Drive Systems and Technologies Conference, IEEE*, Tehran, 2014.
[23] N. Tănase and A. M. Morega, "Radial-axial passive magnetic bearing system Numerical simulation aided design solutions," *The 9th International Symposium on Advanced Topics in Electrical Engineering (ATEE), IEEE*, Bucharest, 2015.
[24] R. Muscia, "Magneto-nechanical model of passive magnetic axial bearings versus the eccentricity error, Part II: Application and results," *The Applied Computational Electromagnetics Society*, vol. 32, no. 8, pp. 678-684, 2017.
[25] A. Mystkowski and E. Pawluszewicz, "Nonlinear position-flux zero-bias control for AMB system with disturbance," *The Applied Computational Electromagnetics Society*, vol. 32, no. 8, pp. 650-656, 2017.
[26] Liuhuijun, "Small axial flux vertical axis wind generators and characteristic research," *Jiaozuo: Henan Polytechnic University*, 2016.

Zhu Jun is engaged in the research of new energy wind power generation and sensorless control theory. Currently, the author has presided over more than 10 provincial projects, published more than 40 academic papers, including more than 20 SCI/EI, application for more than 10 patents. The current projects are: key scientific and technological breakthrough projects in Henan Province: the research of low-speed direct-drive magnetic levitation axial flux wind turbine is conducted from September 2017 to September 2019 with its project number of 182102210052; Henan Colleges special funding for basic scientific research business expenses exploratory project: the vertical moving permanent magnet linear synchronous motor in meta information without sensing control key technology research is conducted from January 2015 to December 2018 with its project number of NSFRF140115. Key project of science and technology research of Henan Provincial Department of Education: the study on the theoretical study of the improved kalman filter permanent magnet synchronous motor without sensor control has been concluded from April 2014 to December 2014 with its project number of 12A470004.

Songdandan is a graduate student, engaged in the design of the magnetic levitation new energy wind generator. There are 6 periodicals, including 2 SCI and EI, whose two patents have been granted.